Electronic Supplementary Material (ESI) for Sensors & Diagnostics.

Synthesis and Characterization of La QDs: Sensor for Anions and H_2O_2

Supplementary information:

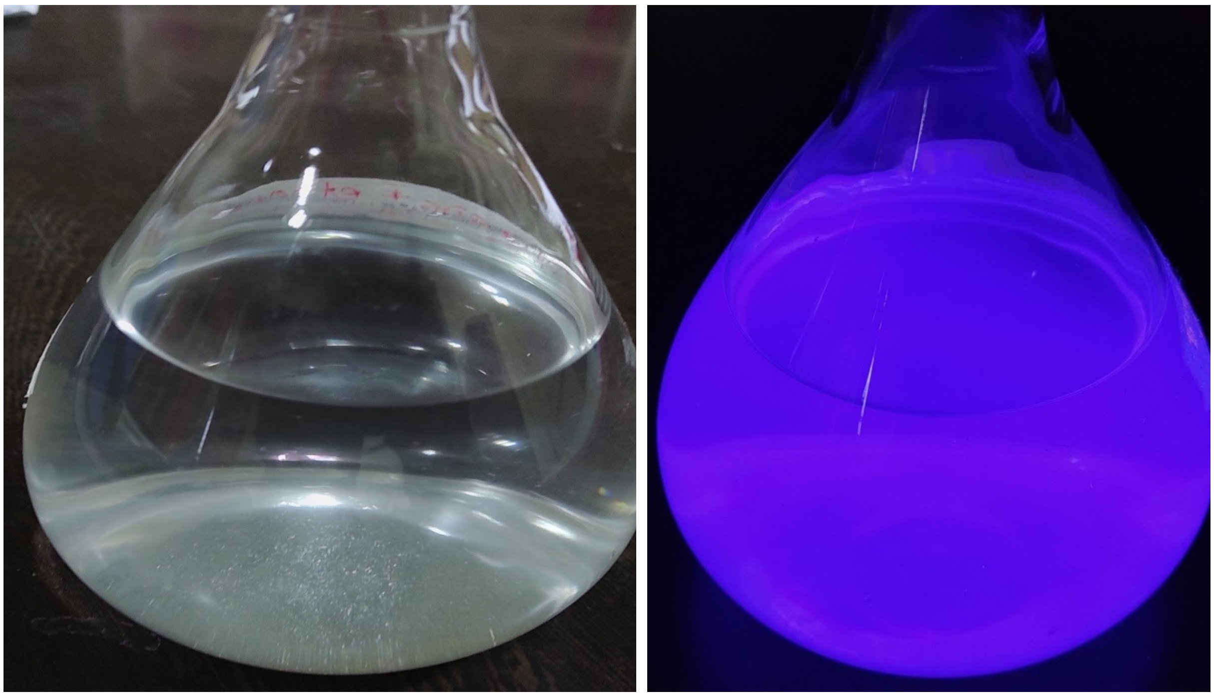

Daylight **UV light**

S1: The visual of the La QDs in ethanol under UV irradiation.

XRD Study:

To find the d-spacing(d) of the XRD peaks Bragg's equation (Equation E1) solution is used at the λ=0.15406nm [38].

$$n\lambda = 2d\, sin(\theta) \qquad \text{(E1)}$$

The lattice constants (a=b=c for cubic, a=b≠c for hexagonal) were calculated by the user of equations E2, and E3 and matched with the standard lattice constants values of the PDF.

Hexagonal crystal lattice constants were calculated by using equationE2.

$$\frac{1}{(d - spacing)^2} = \frac{4(h^2 + k^2 + hk)}{3a^2} + \frac{l^2}{c^2} \qquad \text{(E2)}$$

Cubic crystal lattice constants were calculated by using equation E3.

$$\frac{1}{(d - spacing)^2} = \frac{h^2 + k^2 + l^2}{a^2} \qquad \text{(E3)}$$

By using the Scherrer equation (Equation E4)the crystal grain size (L) was calculated, i.e.

$$L = \frac{k\lambda}{B\ COS(\theta)} \qquad \text{(E4)}$$

where k is a dimensionless shape factor with a typical value of roughly 0.9, is the Bragg angle, λis the X-ray wavelength (0.15406 nm), θ is the wavelength of the X-ray, B is the line whose intensity is halved at maximum intensity (FWHM).

Bandgap energy observation:

The optical band gap energy of the La QDs was calculated through the Tauc plot method (Equation E5).

$$(ahv)^{1/y} = B(hv - E_g) \quad \text{(E5)}$$

where, ν = Photon's frequency,

B = Constant,

h = Planck constant,

Y = ½ or, 2 for direct and indirect transition band gaps, respectively,

Eg = Band gap energy.

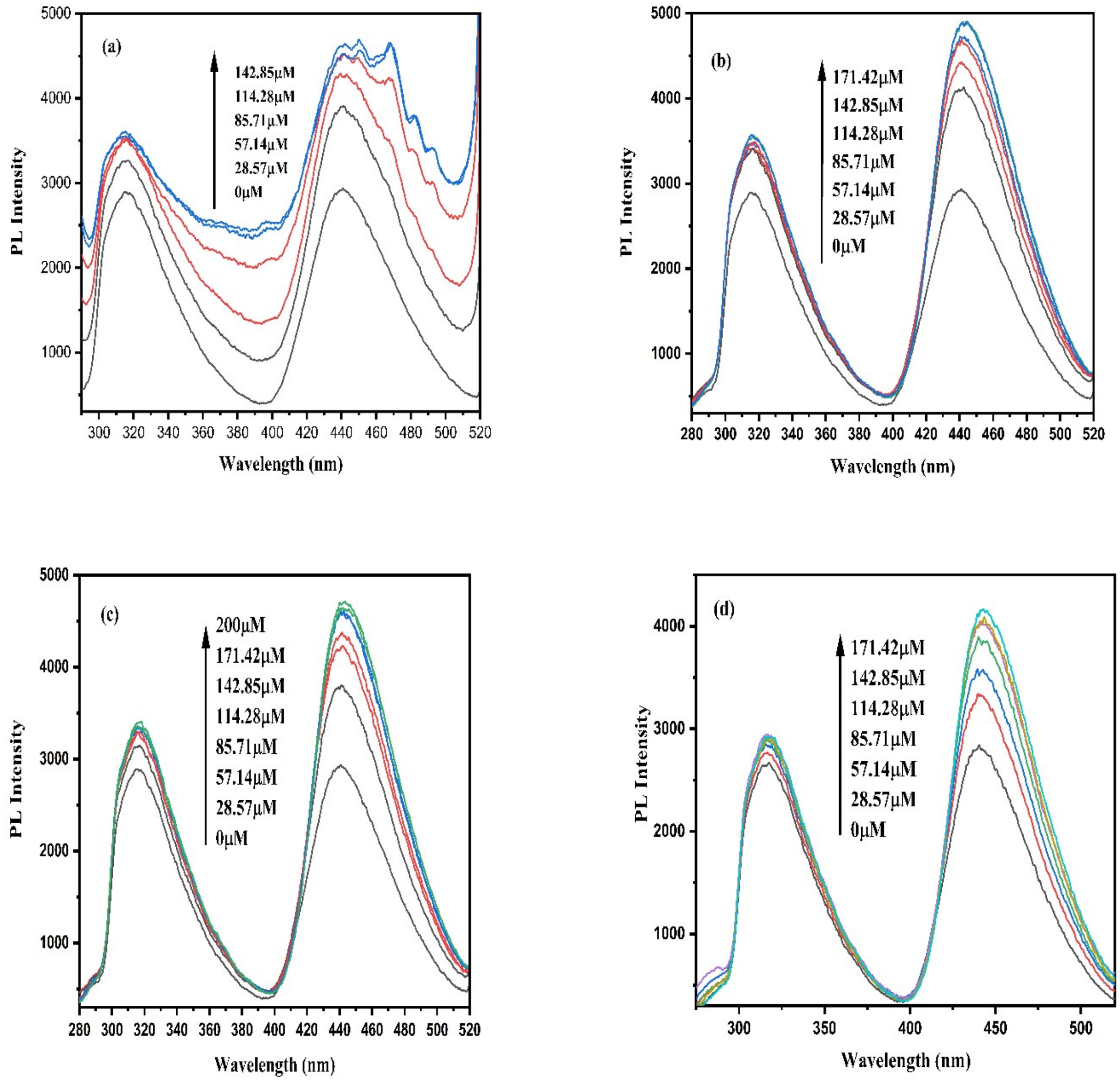

S2: Emission Spectra of the optical La QDs sensor at 315 and 440.5 nm wavelength on excitation at 265nm under different (a) [$C_2O_4^{2-}$], (b) [Br^-], (c) [BrO_3^-], (d) [Cl^-].

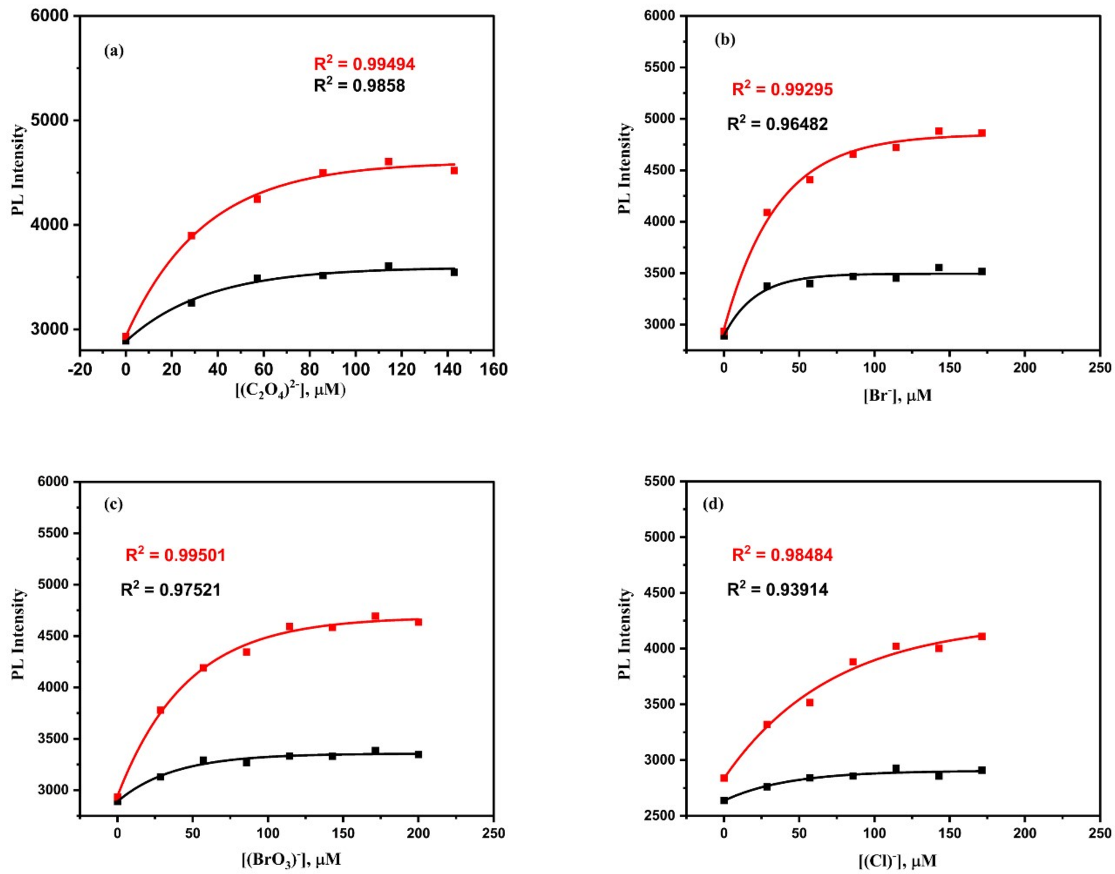

S3: (a) Calibration curves of $C_2O_4^{2-}$sensors peak at 315nm and 440.5 nm wavelengths, (b) Calibration curves of Br^- sensors peak at 315nm and 440.5 nm wavelengths, (c) Calibration curves of BrO_3^- sensors peak at 315nm and 440.5 nm wavelengths, (d) Calibration curves of Cl^- sensors peak at 315nm and 440.5 nm wavelengths.

T1: Calibration curves of F^- sensors peak at 315nm and 440.5 nm wavelengths.

a) At 315nm Peak

Model	Linear
Equation	y = A + Bx
A	2840.97214 ± 30.97025
B	3.38669 ± 0.30065
Residual Sum of Squares	10329.37444
R-Square (COD)	0.96209
Adj. R-Square	0.95451

b) At 440.5nm Peak

Model	Linear
Equation	y = A + Bx
A	2992.715 ± 57.01654
B	11.15023 ± 0.5535
Residual Sum of Squares	35009.54296
R-Square (COD)	0.98783
Adj. R-Square	0.98539

T2: Calibration curves of $(C_2O_4)^{2-}$ sensors peak at 315nm and 440.5 nm wavelengths.

a) At 315nm Peak

Model	Asymptotic
Equation	$y = A - BC^x$
A	3594.77404 ± 36.5841
B	710.10037 ± 51.27378
C	0.97179 ± 0.00535
Reduced Chi-Sqr	1732.88744
R-Square (COD)	0.9858
Adj. R-Square	0.97633

b) At 440.5nm Peak

Model	Asymptotic
Equation	$y = A - BC^x$
A	4603.18656 ± 49.756
B	1668.47565 ± 71.26134
C	0.97094 ± 0.00325
Reduced Chi-Sqr	3399.17413
R-Square (COD)	0.99494
Adj. R-Square	0.99156

T3: Calibration curves of $(CO_3)^{2-}$ sensors peak at 315nm and 440.5 nm wavelengths.

a) At 315nm Peak

Model	Asymptotic
Equation	$y = A - BC^x$
A	3899.83032 ± 123.54159
B	922.03908 ± 143.80652
C	0.98606 ± 0.00593
Reduced Chi-Sqr	15668.78394
R-Square (COD)	0.88463
Adj. R-Square	0.84618

b) At 440.5nm Peak

Model	Asymptotic
Equation	$y = A - BC^x$
A	5594.24238 ± 172.02548
B	2516.96958 ± 259.29451
C	0.98167 ± 0.0048
Reduced Chi-Sqr	58873.90828
R-Square (COD)	0.94069
Adj. R-Square	0.92092

T4: Calibration curves of $(HPO_4)^{2-}$ sensors peak at 315nm and 440.5 nm wavelengths.

a) At 315nm Peak

Model	Asymptotic
Equation	$y = A - BC^x$
A	3418.62035 ± 18.94071
B	528.05859 ± 32.80627
C	0.02206 ± 4.31023E19
Reduced Chi-Sqr	717.50078
R-Square (COD)	0.99661
Adj. R-Square	0.98983

b) At 440.5nm Peak

Model	Asymptotic
Equation	$y = A - BC^x$
A	4669.40318 ± 276.35329
B	1699.14744 ± 361.76002
C	0.94707 ± 0.02518
Reduced Chi-Sqr	65391.77839
R-Square (COD)	0.96045
Adj. R-Square	0.88135

T5: Calibration curves of Br^- sensors peak at 315nm and 440.5 nm wavelengths.

a) At 315nm Peak

Model	Asymptotic
Equation	$y = A - BC^x$
A	3494.59573 ± 27.06847
B	599.59334 ± 57.36622
C	0.95339 ± 0.01227
Reduced Chi-Sqr	2661.52435
R-Square (COD)	0.96482
Adj. R-Square	0.94723

b) At 440.5nm Peak

Model	Asymptotic
Equation	$y = A - BC^x$
A	4850.60968 ± 49.41066
B	1897.31456 ± 80.6551
C	0.97193 ± 0.00303
Reduced Chi-Sqr	5028.61457
R-Square (COD)	0.99295
Adj. R-Square	0.98942

T6: Calibration curves of $(BrO_3)^-$ sensors peak at 315nm and 440.5nm wavelengths.

a) At 315nm Peak

Model	Asymptotic
Equation	$y = A - BC^x$
A	3356.18635 ± 18.56898
B	465.7295 ± 33.23463
C	0.97365 ± 0.00463
Reduced Chi-Sqr	927.16815
R-Square (COD)	0.97521
Adj. R-Square	0.9653

b) At 440.5nm Peak

Model	Asymptotic
Equation	$y = A - BC^x$
A	4684.84755 ± 36.3126
B	1742.30106 ± 55.61913
C	0.97836 ± 0.00175
Reduced Chi-Sqr	2529.38459
R-Square (COD)	0.99501
Adj. R-Square	0.99301

T7: Calibration curves of $(OH)^-$ sensors peak at 315nm and 440.5nm wavelengths.

a) At 315nm Peak

Model	Asymptotic
Equation	$y = A - BC^x$
A	3231.05743 ± 15.2501
B	340.74005 ± 18.67889
C	0.98316 ± 0.00247
Reduced Chi-Sqr	252.43998
R-Square (COD)	0.98656
Adj. R-Square	0.98119

b) At 440.5nm Peak

Model	Asymptotic
Equation	$y = A - BC^x$
A	4374.58031 ± 11.91895
B	1440.90078 ± 15.1365
C	0.98246 ± 4.9002E-4
Reduced Chi-Sqr	170.99122
R-Square (COD)	0.99949
Adj. R-Square	0.99928

T8: Calibration curves of $(Cl)^-$ sensors peak at 315nm and 440.5nm wavelengths.

a) At 315nm Peak

Model	Asymptotic
Equation	$y = A - BC^x$
A	2905.41207 ± 24.71386
B	269.22243 ± 35.1174
C	0.97652 ± 0.00795
Reduced Chi-Sqr	902.02732
R-Square (COD)	0.93914
Adj. R-Square	0.9087

b) At 440.5nm Peak

Model	Asymptotic
Equation	$y = A - BC^x$
A	4245.41798 ± 117.89879
B	1409.41201 ± 115.62499
C	0.98613 ± 0.00297
Reduced Chi-Sqr	4960.76216
R-Square (COD)	0.98484
Adj. R-Square	0.97727

T9: Stern-Volmer plots of F^- sensors peak at 315 and 440.5 nm wavelengths.

a) At 315nm Peak

Model	Stern-Volmer (at 315 nm)
Equation	$I0/I = 1 \pm K_{sv}$ [Q]
K_{sv}	-8.9897E-4 ± 5.19318E-5
Residual Sum of Squares	0.0012
Pearson's r	0.79629
R-Square (COD)	0.9998
Adj. R-Square	0.99977

b) At 440.5nm Peak

Model	Stern-Volmer (at 440.5 nm)
Equation	$I0/I = 1 \pm K_{sv}$ [Q]
K_{sv}	-0.0026 ± 1.49089E-4
Residual Sum of Squares	0.00991
Pearson's r	0.72763
R-Square (COD)	0.99765
Adj. R-Square	0.99726

T10: Stern-Volmer plots of $(C_2O_4)^{2-}$ sensors peak at 315 and 440.5 nm wavelengths.

a) **At 315nm Peak**

Model	Stern-Volmer (at 315 nm)
Equation	$I0/I = 1 \pm K_{sv}$ [Q]
K_{sv}	-0.00172 ± 2.4926E-4
Residual Sum of Squares	0.01395
Pearson's r	0.78499
R-Square (COD)	0.99687
Adj. R-Square	0.99624

b) **At 440.5nm Peak**

Model	Stern-Volmer (at 440.5 nm)
Equation	$I0/I = 1 \pm K_{sv}$ [Q]
K_{sv}	-0.00326 ± 5.03245E-4
Residual Sum of Squares	0.05685
Pearson's r	0.73404
R-Square (COD)	0.98275
Adj. R-Square	0.9793

T11: Stern-Volmer plots of $(CO_3)^{2-}$ sensors peak at 315 and 440.5 nm wavelengths.

a) At 315nm Peak

Model	Stern-Volmer (at 315 nm)
Equation	$I0/I = 1 \pm K_{sv}$ [Q]
K_{sv}	-0.00143 ± 1.63949E-4
Residual Sum of Squares	0.03581
Pearson's r	0.79327
R-Square (COD)	0.99398
Adj. R-Square	0.99323

b) At 440.5nm Peak

Model	Stern-Volmer (at 440.5 nm)
Equation	$I0/I = 1 \pm K_{sv}$ [Q]
K_{sv}	-0.00279 ± 3.73076E-4
Residual Sum of Squares	0.18542
Pearson's r	0.72381
R-Square (COD)	0.94902
Adj. R-Square	0.94265

T12: Stern-Volmer plots of $(HPO_4)^{2-}$ sensors peak at 315 and 440.5 nm wavelengths.

a) At 315nm Peak

Model	Stern-Volmer (at 315 nm)
Equation	$I0/I = 1 \pm K_{sv} [Q]$
K_{sv}	-0.00241 ± 9.71804E-4
Residual Sum of Squares	0.0237
Pearson's r	0.66877
R-Square (COD)	0.99246
Adj. R-Square	0.98994

b) At 440.5nm Peak

Model	Stern-Volmer (at 440.5 nm)
Equation	$I0/I = 1 \pm K_{sv} [Q]$
K_{sv}	-0.00532 ± 0.00161
Residual Sum of Squares	0.0648
Pearson's r	0.59079
R-Square (COD)	0.9732
Adj. R-Square	0.96427

T13: Stern-Volmer plots of Br^- sensors peak at 315nm and 440.5 nm wavelengths.

a) At 315nm Peak

Model	Stern-Volmer (at 315 nm)
Equation	$I0/I = 1 \pm K_{sv} [Q]$
K_{sv}	-0.00138 ± 2.20617E-4
Residual Sum of Squares	0.02169
Pearson's r	0.80087
R-Square (COD)	0.99582
Adj. R-Square	0.99512

b) At 440.5nm Peak

Model	Stern-Volmer (at 440.5 nm)
Equation	$I0/I = 1 \pm K_{sv} [Q]$
K_{sv}	-0.00306 ± 4.59177E-4
Residual Sum of Squares	0.09397
Pearson's r	0.73481
R-Square (COD)	0.97288
Adj. R-Square	0.96836

T14: Stern-Volmer plots of $(BrO_3)^-$ sensors peak at 315nm and 440.5nm wavelengths.

a) At 315nm Peak

Model	Stern-Volmer (at 315 nm)
Equation	$I0/I = 1 \pm K_{sv} [Q]$
K_{sv}	-9.23223E-4 ± 1.21749E-4
Residual Sum of Squares	0.01186
Pearson's r	0.81298
R-Square (COD)	0.99814
Adj. R-Square	0.99788

b) At 440.5nm Peak

Model	Stern-Volmer (at 440.5 nm)
Equation	$I0/I = 1 \pm K_{sv} [Q]$
K_{sv}	-0.00247 ± 3.28232E-4
Residual Sum of Squares	0.08618
Pearson's r	0.75181
R-Square (COD)	0.97927
Adj. R-Square	0.97631

T15: Stern-Volmer plots of $(OH)^-$ sensors peak at 315nm and 440.5nm wavelengths.

a) At 315nm Peak

Model	Stern-Volmer (at 315 nm)
Equation	$I0/I = 1 \pm K_{sv}$ [Q]
K_{sv}	-6.48044E-4 ± 6.84704E-5
Residual Sum of Squares	0.00375
Pearson's r	0.81858
R-Square (COD)	0.99946
Adj. R-Square	0.99938

b) At 440.5nm Peak

Model	Stern-Volmer (at 440.5 nm)
Equation	$I0/I = 1 \pm K_{sv}$ [Q]
K_{sv}	-0.0021 ± 2.47209E-4
Residual Sum of Squares	0.04889
Pearson's r	0.76502
R-Square (COD)	0.98958
Adj. R-Square	0.98809

T16: Stern-Volmer plots of $(Cl)^-$ sensors peak at 315nm and 440.5nm wavelengths.

a) At 315nm Peak

Model	Stern-Volmer (at 315 nm)
Equation	$I0/I = 1 \pm K_{sv}$ [Q]
K_{sv}	-6.75802E-4 ± 8.85997E-5
Residual Sum of Squares	0.0035
Pearson's r	0.81585
R-Square (COD)	0.99943
Adj. R-Square	0.99933

b) At 440.5nm Peak

Model	Stern-Volmer (at 440.5 nm)
Equation	$I0/I = 1 \pm K_{sv}$ [Q]
K_{sv}	-0.00224 ± 2.34541E-4
Residual Sum of Squares	0.02452
Pearson's r	0.75888
R-Square (COD)	0.99442
Adj. R-Square	0.99349

T17: Calibration curves of H_2O_2 sensors peak at 315nm and 440.5nm wavelengths.

a) At 315nm Peak

Model	Asymptotic
Equation	$y = A - BC^x$
A	185.96064 ± 43.05289
B	-3145.85261 ± 45.21972
C	0.89318 ± 0.00407
Reduced Chi-Sqr	1469.89793
R-Square (COD)	0.99882
Adj. R-Square	0.99849

- **At 40˚C**

Model	Asymptotic
Equation	$y = A - BC^x$
A	94.17931 ± 22.1738
B	-1134.2164 ± 20.32908
C	0.91745 ± 0.00376
Reduced Chi-Sqr	163.63192
R-Square (COD)	0.99887
Adj. R-Square	0.99855

b) At 440.5nm Peak

Model	Asymptotic
Equation	$y = A - BC^x$
A	-218.38365 ± 360.5794

B	-4188.00826 ± 327.34836
C	0.94507 ± 0.00863
Reduced Chi-Sqr	9490.90283
R-Square (COD)	0.99355
Adj. R-Square	0.9917

- **At 40˚C**

Model	Asymptotic
Equation	$y = A - BC^x$
A	-52.73118 ± 64.28093
B	-1695.08405 ± 59.06837
C	0.95089 ± 0.00321
Reduced Chi-Sqr	195.30985
R-Square (COD)	0.99909
Adj. R-Square	0.99883

T18: Stern-Volmer plots of H_2O_2 sensors peak at 315nm and 440.5nm wavelengths.

a) At 315nm Peak

Model	Stern-Volmer (at 315 nm)
Equation	$I0/I = 1 \pm K_{sv}$ [Q]
K_{sv}	0.27089 ± 0.01654
Residual Sum of Squares	5.50411
Pearson's r	0.99303
R-Square (COD)	0.97732
Adj. R-Square	0.9748

- **At 40˚C**

Model	Stern-Volmer (at 315 nm)
Equation	I0/I = 1 ±K_{sv} [Q]
K_{sv}	0.15939 ± 0.00748
Residual Sum of Squares	1.12542
Pearson's r	0.99185
R-Square (COD)	0.98936
Adj. R-Square	0.98818

b) At 440.5nm Peak

Model	Stern-Volmer (at 440.5 nm)
Equation	I0/I = 1 ±K_{sv} [Q]
K_{sv}	0.12064 ± 0.00696
Residual Sum of Squares	0.97306
Pearson's r	0.98876
R-Square (COD)	0.98642
Adj. R-Square	0.98491

- **At 40˚C**

Model	Stern-Volmer (at 315 nm)
Equation	I0/I = 1 ±K_{sv} [Q]
K_{sv}	0.09614 ± 0.00486
Residual Sum of Squares	0.47401
Pearson's r	0.9822
R-Square (COD)	0.9912
Adj. R-Square	0.99023

T19: Langmuir binding constants of La QDs for F^-, $C_2O_4^{2-}$, CO_3^{2-}, HPO_4^{2-}, Br^-, BrO_3^-, OH^-, Cl^- ions at the 315nm and 440.5nm wavelengths.

Anions	**$1/I_0$ (315nm wavelength)**	**Slope from Langmuir description fitting (315nm wavelength)**	**Intercept**	**Binding constant(B) (315nm wavelength)**	**$1/I_0$ (440.5nm wavelength)**	**Slope from Langmuir description fitting (440.5nm wavelength)**	**Intercept**	**Binding constant(B) (440.5nm wavelength)**
F^-	3.45956×10^{-4}	$2.90815\times10^{-4}\pm 7.01925\times10^{-6}$	$0.00143 \pm 7.23057\times10^{-4}$	$0.20337 (\pm 0.97 \times 10^{-2})$	3.40842×10^{-4}	$2.03226\times10^{-4}\pm 1.096\times10^{-5}$	0.0024 ± 0.00113	$0.08468 (\pm 0.96 \times 10^{-2})$
$C_2O_4^{2-}$	3.45956×10^{-4}	$2.7806\times10^{-4}\pm 3.37839\times10^{-6}$	$3.84804\times10^{-4}\pm 2.92231\times10^{-4}$	$0.7226 (\pm 1.15 \times 10^{-2})$	3.40842×10^{-4}	$2.16028\times10^{-4}\pm 4.54463\times10^{-6}$	$6.08957\times10^{-4}\pm 3.9311\times10^{-4}$	$0.35475 (\pm 1.15 \times 10^{-2})$
CO_3^{2-}	3.45956×10^{-4}	$2.52658\times10^{-4}\pm 5.43355\times10^{-6}$	$0.00148 \pm 7.39093\times10^{-4}$	$0.17071 (\pm 0.73 \times 10^{-2})$	3.40842×10^{-4}	$1.71523\times10^{-4} \pm 5.2722\times10^{-6}$	$0.00173 \pm 7.17146\times10^{-4}$	$0.09915 (\pm 0.73 \times 10^{-2})$
HPO_4^{2-}	3.45956×10^{-4}	$2.90869\times10^{-4} \pm 7.99597\times10^{-7}$	$2.94383\times10^{-5} \pm 3.65687\times10^{-5}$	$9.88063 (\pm 2.18 \times 10^{-2})$	3.40842×10^{-4}	$2.09423\times10^{-4} \pm 7.6377\times10^{-6}$	$4.29545\times10^{-4} \pm 3.49302\times10^{-4}$	$0.48755 (\pm 2.18 \times 10^{-2})$
Br^-	3.45956×10^{-4}	$2.8243\times10^{-4} \pm 2.58782\times10^{-6}$	$3.66365\times10^{-4} \pm 2.66573\times10^{-4}$	$0.7709 (\pm 0.97 \times 10^{-2})$	3.40842×10^{-4}	$2.01963\times10^{-4} \pm 3.67487\times10^{-6}$	$8.42041\times10^{-4} \pm 3.78551\times10^{-4}$	$0.23985 (\pm 0.97 \times 10^{-2})$
BrO_3^-	3.45956×10^{-4}	$2.95989\times10^{-4} \pm 1.91713\times10^{-6}$	$4.33998\times10^{-4} \pm 2.29134\times10^{-4}$	$0.68201 (\pm 0.83 \times 10^{-2})$	3.40842×10^{-4}	$2.10252\times10^{-4} \pm 3.48048\times10^{-6}$	$0.00105 \pm 4.15984\times10^{-4}$	$0.20024 (\pm 0.83 \times 10^{-2})$
OH^-	3.45956×10^{-4}	$3.09443\times10^{-4} \pm 1.74903\times10^{-6}$	$4.48558\times10^{-4} \pm 2.09043\times10^{-4}$	$0.68986 (\pm 0.83 \times 10^{-2})$	3.40842×10^{-4}	$2.26718\times10^{-4} \pm 3.55396\times10^{-6}$	$0.0012 \pm 4.24766\times10^{-4}$	$0.18893 (\pm 0.83 \times 10^{-2})$
Cl^-	3.79003×10^{-4}	$3.43745\times10^{-4} \pm 2.93487\times10^{-6}$	$3.04169\times10^{-4} \pm 3.02323\times10^{-4}$	$0.20337 (\pm 0.97 \times 10^{-2})$	3.52149×10^{-4}	$2.39308\times10^{-4} \pm 5.9718\times10^{-6}$	$0.00131 \pm 6.15159\times10^{-4}$	$0.08468 (\pm 0.97 \times 10^{-2})$